Highly Acid–Resistant, Magnetically Steerable Acoustic Micromotors Prepared by Coating Gold Microrods with Fe3O4 Nanoparticles via pH Adjustment

8 authors, including:

Chao Zhou
Harbin Institute of Technology Shenzhen Graduate School
15 PUBLICATIONS   **85** CITATIONS

SEE PROFILE

Xiao-Hui Yan
The Chinese University of Hong Kong
43 PUBLICATIONS   **397** CITATIONS

SEE PROFILE

Li Zhang
Guangzhou Medical University
145 PUBLICATIONS   **1,795** CITATIONS

SEE PROFILE

Wei Wang
Harbin Institute of Technology (Shenzhen)
30 PUBLICATIONS   **1,605** CITATIONS

SEE PROFILE

Some of the authors of this publication are also working on these related projects:

Editorial for the special issue on micro-/nanorobotics View project

Nano-patterned SU-8 surface using nanosphere-lithography for enhanced neuronal cell growth View project

**ADVANCED
SCIENCE NEWS**

www.advancedsciencenews.com

Particle
& Particle Systems Characterization

www.particle-journal.com

FULL PAPER

Highly Acid-Resistant, Magnetically Steerable Acoustic Micromotors Prepared by Coating Gold Microrods with Fe₃O₄ Nanoparticles via pH Adjustment

Zeheng Li, Lanjun Bai, Chao Zhou, Xiaohui Yan, Lamar Mair, Anning Zhang, Li Zhang, and Wei Wang*

There is mounting interest in designing magnetically steerable nano- and micromotors for next generation medical nanorobotics, which requires biocompatibility for each individual component. Although various magnetic materials (e.g., Ni, Co, and Fe₃O₄) have been incorporated into micromotors, their acid resistance remains largely unexplored. In this article, a simple one-step method to prepare magnetic microrods via electrostatic attraction between paramagnetic magnetite nanoparticles (Fe₃O₄ NPs) and gold microrods at appropriate pH values is reported. The as-prepared Fe₃O₄-coated micromotors can be powered by MHz ultrasound and easily steered by external magnetic fields, and perform well in harsh working conditions such as high acidity, high viscosity, and high ionic strength. In particular, extended exposure to solution of pH as low as 0.9 has a minimal effect on the speed, steerability, or cargo-transporting capability of micromotors coated with Fe₃O₄ NPs, in stark contrast with those containing Ni segments. Considering the many challenges of biomedical applications, acid-resistant, magnetically steerable Fe₃O₄-coated micromotors powered by MHz ultrasound can be a promising prototype for the future development of medical nano- and microrobotics.

1. Introduction

Medical nano- and microrobotics, long envisioned in popular fantasies such as Fantastic Voyage, have recently received a significant amount of interest.[1–5] As a key step toward realizing this dream, various propulsion and steering techniques have

Z. Li, L. Bai, C. Zhou, A. Zhang, Prof. W. Wang
School of Material Sciences and Engineering
Harbin Institute of Technology
Shenzhen Graduate School
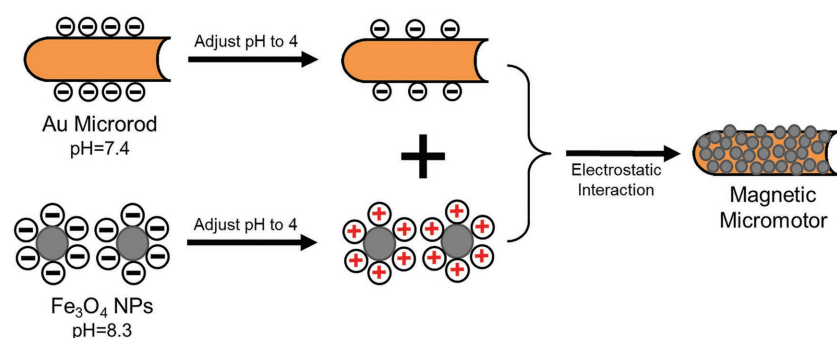Shenzhen 518055, China
E-mail: wwang@hitsz.edu.cn
Dr. X. Yan, Prof. L. Zhang
Department of Mechanical and Automation Engineering
The Chinese University of Hong Kong
Shatin, N.T., Hong Kong SAR 999077, China
Dr. L. Mair
Weinberg Medical Physics LLC Bethesda
Bethesda, MD 20817, USA
Prof. W. Wang
Center for Soft and Living Matters
Institute of Basic Sciences
Ulsan 44919, Korea

enabled synthetic colloidal particles to move autonomously.[6–10] These micromotors, typically hundreds of nanometers to several micrometers in size, can be powered by chemical reactions and/or gradients,[10–19] thermal gradients,[20–24] electromagnetic fields (including light),[25–31] and ultrasound,[32,33] and move with speeds up to hundreds body lengths per second.[19] Building upon such mobility, initial applications include sensing,[34,35] environmental remediation,[36–39] microassembly,[40] and biomedicine.[41–44] Ultrasound, due to its biocompatible nature, has seen an increasing interest in being used as one of the power sources for future medical nanorobots.[45]

Although we are encouraged by a few early reports on the in vivo application of these micromachines,[46,47] formidable biological challenges call for designs of higher power output, better controllability, and more versatile functionalities.[48,49] In particular, the task of monitoring and controlling micromotors once they are in the complex maze of human bodies remains a major challenge.[50,51] One envisioned approach is to use chemotaxis to guide synthetic micromotors, mimicking a method mammalian and bacterial cells regularly use for navigation;[52] chemotaxis methods, however, have seen little progress in real applications.[53–57] Alternatively, external steering of magnetic micromotors offers a more controlled method of guidance, and has the potential to be broadly applicable (see recent review and the references therein).[58,59] Conventionally, nickel (Ni) or cobalt (Co) coatings or segments have been widely used as magnetic layers to enable steering, as they can be incorporated into micromotor structures via physical or chemical deposition. However, Ni and Co are known to be highly chemically active and unstable in acidic environments. Such reactivity is particularly detrimental in biomedical applications involving low pH environments. For example, drug delivery to tumors and operations in stomach are scenarios in which Ni or Co coatings might dissolve and lead to loss of magnetic steerability, as well as possibly toxic side effects from nickel and cobalt ions.

Magnetite (Fe₃O₄), on the other hand, is of low cytotoxicity,[60,61] resists proton attack more effectively than active metals such as Ni or Co, and has magnetic properties suitable for steering magnetic micromotors. Along this line, micromotors

Scheme 1. One-step fabrication of Fe$_3$O$_4$-coated gold microrods by adjusting solution pH. Gold rods and Fe$_3$O$_4$ nanoparticles are not shown to scale.

metal rods: (1) surface charges of colloidal particles in water are subject to change at different solution pH; and (2) strong electrostatic interactions tend to bind two oppositely charged colloidal particles. Conventionally, Fe$_3$O$_4$ NPs are coated onto other particles by chemically functionalizing either surface so the surfaces carry opposite charges; electrostatic attraction then leads to aggregation of NPs on the surface. Herein, we circumvent the time-consuming intermediary binding chemistry, and simply tune the sign and magnitude of surface charges on Fe$_3$O$_4$ NPs and gold microrods by varying solution pH. By doing so, opposite charges are induced on the surfaces of both particles, which then spontaneously bind to each other (Scheme 1).

Following these simple design principles, uniform coating of Fe$_3$O$_4$ NPs on gold microrods was successfully achieved at pH 4. Magnetite nanoparticles (Fe$_3$O$_4$ NPs) of ≈10 nm were synthesized by a co-precipitation method (**Figure 1**a,b, see Figure S1, Supporting Information, for magnetic characterization).[67] Gold microrods ≈2 µm in length and ≈300 nm in diameter were synthesized by template-guided electrodeposition (Figure 1c).[68] Zeta potentials of Fe$_3$O$_4$ NPs and gold microrods, as a function of solution pH, are shown in Figure 1e. Fe$_3$O$_4$ NPs at neutral pH carry slight negative charges (≈−20 mV) on the surface, but their zeta potentials become increasingly negative when pH is increased beyond 7. In acidic environment the Fe$_3$O$_4$ NP surface is protonated and carry positive charges, peaking at ≈60 mV at pH 4. Similar change of zeta potential of bare Fe$_3$O$_4$ NPs as a function of solution pH has been previously reported, and is attributed to the following surface reactions[69]

with Fe$_3$O$_4$ either coated on the surface or embedded inside the micromotor have recently been designed,[40,60,62–66] but with little performance comparison with Ni-containing micromotors in acidic environments. Moreover, incorporating Fe$_3$O$_4$ into/onto the micromotor is also relatively costly that could involve hypotonic dilution encapsulation method,[62] biotemplating process,[63] or chemical deposition.[40,60,64–66] In this article we report a simple, fast, inexpensive, and effective way to prepare Fe$_3$O$_4$-coated metal microrods as magnetically steerable ultrasound micromotors, by exploiting differences in microrod and nanoparticle surface charges at various pH values (**Scheme 1**). We show that the Fe$_3$O$_4$ coating not only imparts magnetic steerability to the acoustic micromotor without compromising its speed but also able to withstand highly acidic solutions, comparing favorably to similar rods with Ni segments. Further experiments in fluids of high viscosity and high ionic strength suggest Fe$_3$O$_4$-coated ultrasound micromotors could be useful as biocompatible micromachines.
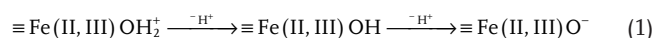
2. Results and Discussions

2.1. Fabrication of Fe$_3$O$_4$-Coated Gold Microrods

Two simple and well-established concepts are considered when designing an effective strategy for coating Fe$_3$O$_4$ NPs onto

$$\equiv Fe\,(II, III)\,OH_2^+ \xrightarrow{\;-H^+\;} \equiv Fe\,(II, III)\,OH \xrightarrow{\;-H^+\;} \equiv Fe\,(II, III)\,O^- \qquad (1)$$

On the other hand, gold microrods carry negative charges at all pH values we tested (pH 2 through pH 12), and microrod zeta potential reaches a minimum of ≈−80 mV at pH 8. Taking advantage of the opposite charges on Fe$_3$O$_4$ NPs and microrods,
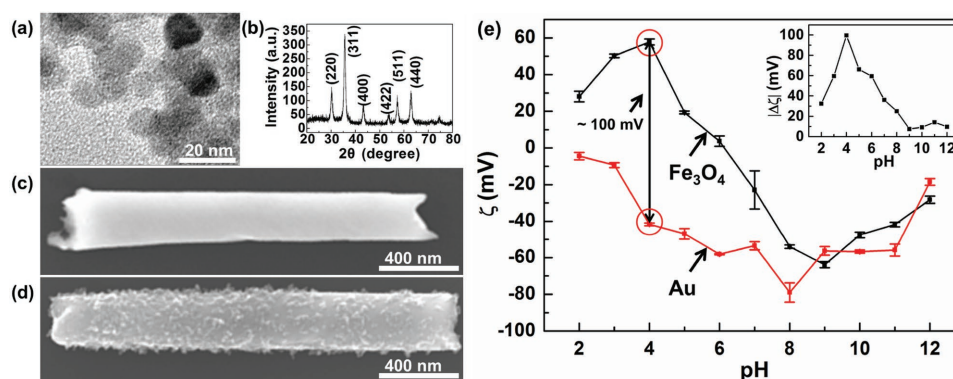
Figure 1. Fabrication of Fe$_3$O$_4$-coated gold microrods. a,b) Transmission electron microscopy image and X-ray diffraction patterns of the synthesized Fe$_3$O$_4$ NPs. Scanning electron microscopy images of the synthesized gold microrods c) before and d) after Fe$_3$O$_4$ coating. e) Zeta potential measurement of synthesized Fe$_3$O$_4$ NPs and gold microrods at various pH. Inset: Difference in zeta potential between these two particles at different pH, maximizing around pH = 4.

ADVANCED
SCIENCE NEWS
www.advancedsciencenews.com

Particle
& Particle Systems Characterization
www.particle-journal.com

FULL PAPER

and the ≈100 mV difference in zeta potential at pH 4, we attached Fe_3O_4 NPs to the surfaces of gold microrods through electrostatic attraction and formed a dense, magnetic layer on the microrods (Figure 1d). Mixing these two types of particles at other non-optimal pH resulted in only partial coverage of microrods with Fe_3O_4 NPs (scanning electron microscopy (SEM) images of Fe_3O_4-coated gold rods produced at pH = 2 and 3 are shown in Figure S2, Supporting Information). We note that the bond between Fe_3O_4 NPs and gold surface is functionally irreversible; no Fe_3O_4 NP detachment from the rods was observed. Even strong agitation such as that by ultrasonic cleaning bath for 10 min did not result in any appreciable change in the behaviors of microrods coated with Fe_3O_4 NPs. These Fe_3O_4-coated gold microrods prepared at pH = 4 were used for all subsequent experiments, where their magnetic steerability and performance as ultrasound powered micromotors are further tested.

2.2. Performance of Gold Rods in Ultrasound with and without Magnetic Coating

Recently, megahertz (MHz) frequency standing waves have been used to propel metallic microrods into fast and directional motion in water.[33] The attachment of magnetic Fe_3O_4 NPs imparts magnetic susceptibility to otherwise non-magnetic gold microrods, enabling us to steer the microrods under ultrasound propulsion via external magnetic fields (permanent magnets, see **Figure 2**a for the experiment setup). We demonstrate this steering capability through a series of tests. First, we note in Figure 2 and Video S1 (Supporting Information) a clear change in the trajectories of ultrasonically propelled gold microrods with or without magnetic steering (Figure 2b,c): the tightly circular motion of rods changed to linear motion with large persistence length when the magnetic field was applied. Alternating "circular-linear-circular" motion of multiple motors due to momentary application of the magnetic field can be found in Video S2 (Supporting Information). Changes in microrod trajectory was further quantified by calculating the directionality of the moving rods. The directionality is defined as the average of $\cos\Delta\theta$ of many steps, where $\Delta\theta$ is the difference in angle between the velocity vectors of every two steps along the micromotor trajectory (see Figure S7, Supporting Information, for details).[70] A significant change in directionality from 0.48 ± 0.30 (very circular) to 0.99 ± 0.06 (almost linear) before

and after magnetic steering was found for an ensemble of rods. Such an abrupt change in directionality in the presence of magnetic steering is very similar to that demonstrated by microrods containing Ni segments, both from previous reports[71] and our own experiments (see Figures S8–S10, Supporting Information). However, due to the ferromagnetic nature of Ni (see, e.g., the hysteresis loop from **Figure 3**b[71]), microrods containing Ni segments tended to aggregate into small clusters as a result of magnetic interactions during and after magnetic steering. Such aggregation, however, was not observed for microrods coated with paramagnetic Fe_3O_4 NPs, consistent with the negligible remanence of Fe_3O_4 NPs when the magnetic field was turned off (Figure S1, Supporting Information). The other difference in magnetic steering between paramagnetic Fe_3O_4 and ferromagnetic Ni (or Co) was that the former aligns the particle parallel to the field lines while the latter perpendicular.[64] However, this is trivial in our experiment since the magnetic field can be easily rotated to produce any alignment. In fact, this is exploited to guide the micromotors to write arbitrary letters by continuously adjusting the orientation of the magnets (see TOC figure and Video S3 (Supporting Information), where letters "HIT" and numbers "1920–2016" were written by acoustic micromotors).

We emphasize that the Fe_3O_4 coating as well as magnetic steering cause minimal change to the speed of the ultrasonically propelled microrods, and negligibly affects micromotor performance as a function of transducer voltage and frequency (see Figures S3–S6, Supporting Information, for details). Such a lack of change in performance is interesting in its own way, and might help us understand the propulsion mechanism of microrods in MHz ultrasound. A popular hypothesis regarding the mechanism suggests that shape asymmetry of the particle in ultrasound plays a significant role in determining micromotor translational velocities.[33,71–74] This effect likely originates from the concavity near the microrod tips due to fabrication imperfection, with a feature size on the order of 100 nm. The Fe_3O_4 NPs we synthesized are, however, about one order of magnitude smaller, and therefore when attached to the microrod surface might not be enough to alter its shape asymmetry or modulates the micromotor's speed. This appears to agree well with the theoretical prediction from Nadal and Lauga that the speed of an ultrasound-powered motor is critically dependent on the size of the asymmetric features.[75] A more quantitative study on this matter, although important, is not a focus of the current work, and therefore will be pursued separately.
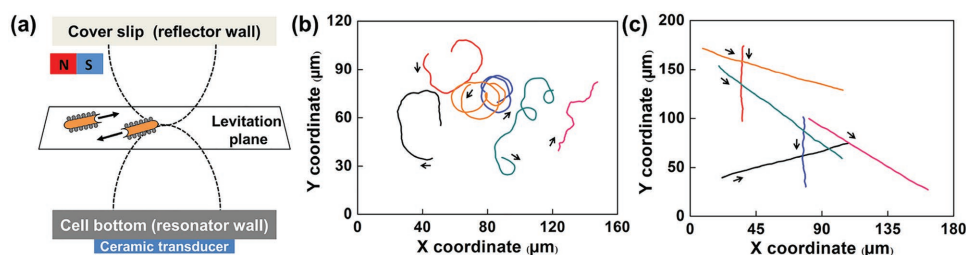
Figure 2. Control and manipulation of Fe_3O_4-coated ultrasound micromotors. a) Scheme of ultrasound experiment. The metal rods are added for artistic illustration purpose, and are not to scale. Actual trajectories of an ensemble of ultrasound micromotors in Video S1 (Supporting Information) when the field is b) off and c) on. The average directionality of the ensemble ($\cos\Delta\theta$) changes from 0.48 to 0.99 when the field is applied. A total of six motors were tracked and color coded, and the same colors in (b) and (c) represent the same motors before and during magnetic steering.
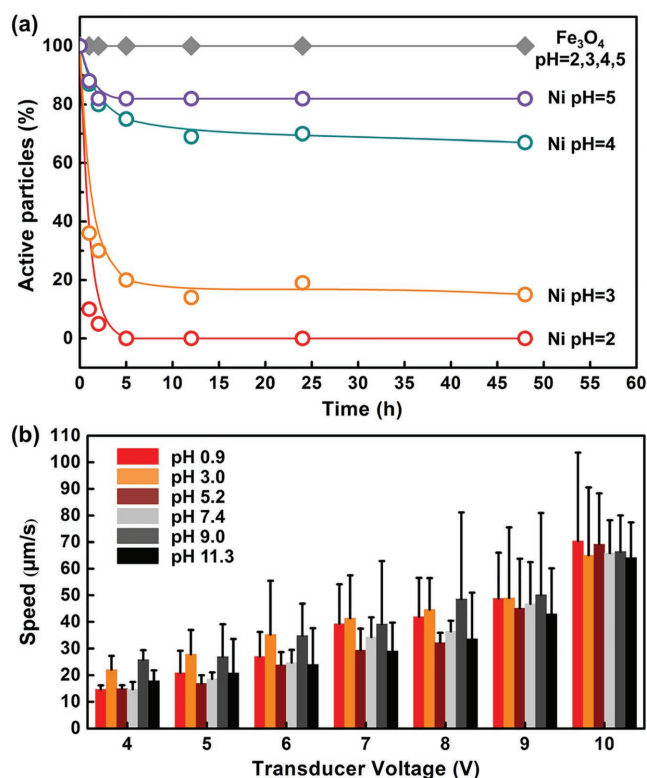
Figure 3. Performance of Fe$_3$O$_4$ NP-coated and Ni-containing gold microrods in solutions at various pH. a) Responsiveness of two types of microrods to a magnetic field after exposure to solutions of pH ranging from 2 to 5 for up to 48 h. b) The speed of Fe$_3$O$_4$-coated motors at different transducer voltages in solutions of pH ranging from 0.9 to 11.3. For any particular voltage the data are arranged with low pH on the left and high pH on the right. Error bars are the standard deviation of measurement of more than ten individual micromotors.

2.3. Magnetic Micromotors in Biologically Relevant Environments

Having confirmed the magnetic steerability of Fe$_3$O$_4$ NP-coated gold microrods, we now examine in vitro their performance in three aspects relevant to the successful operation of medical nano-robots: chemical stability in acidic environments,

swimming performance in body fluids, and cargo delivery capability. By doing so, we highlight the usability as well as limitations of ultrasonically propelled micromotors in future biomedical applications, which have been one of the major motivations behind the development of nano- and micromachines.

2.3.1. Magnetic Micromotors in Acids

One of the major benefits of Fe$_3$O$_4$ NPs as a magnetic coating versus nickel is its resistance to acids, which is critical for the operation of medical nanorobots in acidic environments such as tumors (pH as low as ≈6)[76] and digestive tracts (pH from 1–3). The excellent resistance to acid of Fe$_3$O$_4$ NP-coated micromotor is characterized and confirmed in this section. To be specific, we mixed both Fe$_3$O$_4$ NP-coated gold microrods (i.e., the "test subject") and gold-nickel segmented microrods (i.e., the "control," with Ni segment ≈500 nm long) in solutions with pH ranging from 2 to 5 for up to 48 h. The responsiveness of these motors to a magnetic field was tested after the acid treatment, and the results are plotted in Figure 3. It is clear that nickel-containing micromotors suffered significant degradation in acids, rendering them nearly unresponsive to magnetic fields after 4 h of acidic treatment at pH 2. Fe$_3$O$_4$-coated motors, on the other hand, remained highly responsive to magnetic fields even after extended exposure to highly acidic solutions (48 h at pH 2). Finally, Fe$_3$O$_4$-coated motors maintained the same level of magnetic steerability even after being immersed in solution of pH 0.9 for 24 h, demonstrating an impressive level of robustness and reliability that is suitable for extreme in vivo conditions. Fe$_3$O$_4$ NPs were found to be partially etched away when exposed to solutions of pH 0.9 for more than 72 h.

2.3.2. Magnetic Micromotors in Fluids of High Viscosity and Ionic Strength

Body fluids are complex environments with high ionic strength (on the order of 1 mol L^{-1}), and viscosities substantially higher than pure water. It is therefore necessary to assess the performance of acoustic micromotors in similar conditions in vitro. To this end, we compared the speed of Fe$_3$O$_4$-coated gold microrods in deionized water with that in a number of fluids (**Figure 4**), including phosphate buffered saline (PBS) solution,
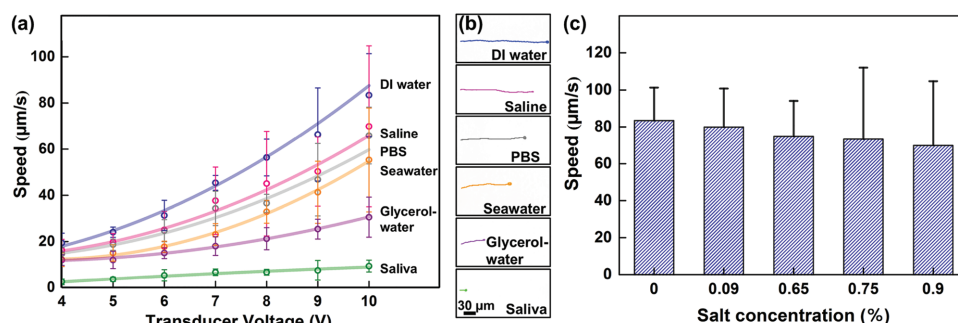
Figure 4. Performance of Fe$_3$O$_4$-coated ultrasound micromotors in various fluids. a) Speeds of micromotors at various driving voltages in water, saline, PBS buffer solution, seawater (90% v/v), glycerol-water 1:1 mixture, and saliva (20% v/v). Solid lines are hyperbolic fits.[72] b) Representative trajectories of micromotors steered by magnets moving in the above six fluids at 10 V. c) Speeds of micromotors in saline solutions of various concentrations. 0.9% saline solution contains 0.15 mol L^{-1} Na$^+$ ions and 0.15 mol L^{-1} Cl$^-$ ions. Error bars are the standard deviation of measurement of more than 20 individual micromotors.

**ADVANCED
SCIENCE NEWS**

www.advancedsciencenews.com

Particle
& Particle Systems Characterization

www.particle-journal.com

FULL PAPER

solutions of various salt concentrations, sea water (90% v/v), saliva (20% v/v), and a 50% glycerol–water mixture (viscosity ≈ 7 mPa s). The results show a clear decrease in motor speed when they are placed in fluids of high viscosity as compared to that in pure water. This is relatively easy to understand, given the drag force is inversely proportional to viscosity (a more comprehensive study on this effect will be published separately). A previous report with Ni containing acoustic micromotor showed very similar speed values and trends in the same tested liquids.[73] We note that varying the fluid viscosity inevitably changes the speed of sound in the medium, and we have monitored such change and made certain the corresponding resonance frequency was always used. On the other hand, the effect of ions on the speed of ultrasonically propelled microrods is quite small (within errors, Figure 4c), consistent with the negligible change in acoustic radiation force at different salt concentrations (see Equations (S1) and (S2), Supporting Information, for a rough estimate).

2.3.3. Cargo Delivery by Magnetic Micromotors

Finally, we demonstrate cargo pickup, transport, and release by Fe_3O_4 NP-coated gold microrods (**Figure 5**, and Video S4, Supporting Information). These rods can readily pick up nearby magnetic microbeads (urea-formaldehyde magnetic beads, 0.89 μm in diameter) via magnetic interactions, and unload them at will by a sudden turn of the magnetic field (therefore a turn of the motor). Due to increased drag, motor-cargo duos moved at an average speed ≈54% of the speed of unladen micromotors. In addition, more than one cargo can be loaded by subsequent magnetic attraction (see Video S5, Supporting Information). Significantly, the ability to perform cargo pickup and delivery using Fe_3O_4 NP-coated acoustic micromotor is retained after incubation in pH 3 solution for 24 h. By comparison, the Ni-containing micromotors completely lost such capability as a result of Ni degradation in acids.

3. Conclusion

To summarize, we have demonstrated that magnetically steered, ultrasound-powered micromotors can be easily prepared by electrostatic attraction between Fe_3O_4 NPs and gold microrods at appropriate pH values. This method circumvents the need for chemically functionalizing either particle surface or physically depositing Fe_3O_4, and produces micromotors with uniform magnetic coatings. These coatings had minimal effect on the acoustic propulsion of microrods, while imparting excellent magnetic steerability, which is evident in the linear trajectories in the presence of a magnetic field. Importantly, we showed that Fe_3O_4-coated micromotors performed well in a wide range of working conditions that are relevant to biological applications, such as high acidity, high viscosity, and high ionic strength. Solution pH as low as 0.9 had a minimal effect on the speed, steerability, or cargo-transporting capability of Fe_3O_4-coated micromotors, in stark contrast with those containing Ni as the magnetic segment. In addition, unlike ferromagnetic Ni coating that induces particle aggregation, the paramagnetic nature of Fe_3O_4 nanoparticles promises much easier handling of micromotors. Considering the many challenges presented by in vivo biomedical applications, we believe Fe_3O_4-coated micromotors powered by MHz ultrasound can be a promising prototype for the future development of medical nano- and microrobotics.

4. Experimental Section

Synthesis of Fe_3O_4 Nanoparticles: $FeCl_3·6H_2O$ (0.541 g) and $FeCl_2·4H_2O$ (0.200 g) were added into 50 mL of previously degassed deionized water, and the mixture was stirred for 1 min. Then 2 mL of fresh ammonia was added during vigorous mixing. The reaction mixture was kept at 70 °C in water bath for 1 h, and then allowed to cool down to room temperature. Nitrogen gas was flown into the reaction mixture throughout the entire synthesis. Fe_3O_4 nanoparticles were separated from the suspension by a permanent magnet and rinsed by deionized water at least three times. The pH value of aqueous Fe_3O_4 suspension slowly increases until stabilizing around 8.3.
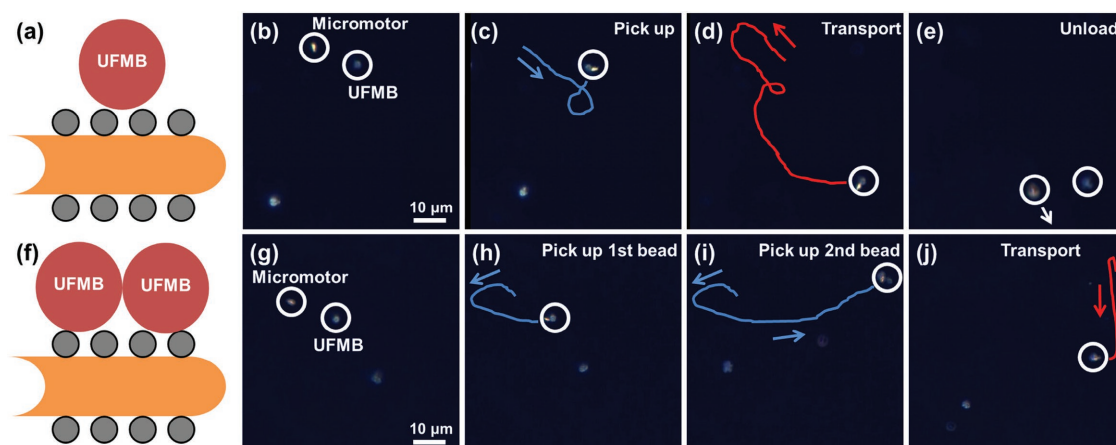
Figure 5. Loading, transport, and unloading of magnetic microparticles (UFMB) by Fe_3O_4-coated gold micromotors (snapshots from Videos S4 and S5, Supporting Information). a–e) The whole process for one cargo, and f–j) two cargos can be subsequently loaded and transported. Cartoons in (a) and (f) are not drawn to scale.

FULL PAPER

Synthesis of Gold Microrods: Metal microrods were synthesized by a template-assisted electrodeposition in porous anodized alumina membranes (AAO, nominal pore size ≈200 nm, Whatman) following previous protocols.[77,78] In general, silver was thermally evaporated on one side of the membrane to serve as the electrical contact. Then silver (≈10 μm) was electrodeposited into the membrane pores at negative currents. Gold was deposited after silver, and an optional nickel segment can be grown after that. The length of each segment was controlled by the amount of charge passing through the electrochemical cell. Microrods were released from the membrane by first dissolving the silver layers in diluted nitric acid, followed by dissolving the AAO membrane in NaOH solutions.

Ultrasound Actuation Experiment: The ultrasound actuation experiments were conducted in a similar way to previous reports.[33] The setup was constructed based on Figure 2a, by attaching a few layers of Kapton tape on a piece of silicon wafer, on the back of which a piece of PZT ceramic disk was glued (Steminc, Part No. SMD12T06R412WL) by epoxy resin. A circular hole of ≈200 μm in height and ≈5 mm in diameter was cut on the Kapton tape to serve as the acoustic cell. During the experiment, a function generator (Agilent 33210A) sends an ≈3 MHz sinusoidal signal to the piezoelectric disk, which produces ultrasound that propagates through the microparticle suspension in the acoustic cell. At the resonance frequency, metal particles floated up to the levitation plane at the center of the acoustic cell and moved. Their trajectories were recorded by a CCD camera (Point Grey) mounted on an upright optical microscope at 30 frames s^{-1}, and analyzed by standard particle tracking algorithms via Matlab. Magnetic steering was achieved by a handheld NdFeB permanent magnet.

Supporting Information

Supporting Information is available from the Wiley Online Library or from the author.

Acknowledgements

[1] T. E. Mallouk, A. Sen, *Sci. Am.* **2009**, *300*, 72.

[2] J. J. Abbott, M. C. Lagomarsino, L. Zhang, L. Dong, B. J. Nelson, *Int. J. Rob. Res.* **2009**, *28*, 1434.

[3] B. J. Nelson, I. K. Kaliakatsos, J. J. Abbott, *Annu. Rev. Biomed. Eng.* **2010**, *12*, 55.

[4] G. A. Ozin, I. Manners, S. Fournier-Bidoz, A. Arsenault, *Adv. Mater.* **2005**, *17*, 3011.

[5] S. Martel, *IEEE Spectrum* **2012**, *49*, 48.

[6] a) S. Sanchez, L. Soler, J. Katuri, *Angew. Chem.* **2015**, *127*, 1432; b) *Angew. Chem. Int. Ed.* **2015**, *54*, 1414.

[7] M. Guix, C. C. Mayorga-Martinez, A. Merkoçi, *Chem. Rev.* **2014**, *114*, 6285.

[8] I. S. Aranson, *Phys.-Usp.* **2013**, *56*, 79.

[9] S. Ebbens, *Curr. Opin. Colloid Interface Sci.* **2016**, *21*, 14.

[10] W. Wang, W. Duan, S. Ahmed, T. E. Mallouk, A. Sen, *Nano Today* **2013**, *8*, 531.

[11] J. R. Howse, R. A. Jones, A. J. Ryan, T. Gough, R. Vafabakhsh, R. Golestanian, *Phys. Rev. Lett.* **2007**, *99*, 048102.

[12] W. F. Paxton, K. C. Kistler, C. C. Olmeda, A. Sen, S. K. St. Angelo, Y. Cao, T. E. Mallouk, P. E. Lammert, V. H. Crespi, *J. Am. Chem. Soc.* **2004**, *126*, 13424.

[13] J. Gibbs, Y. P. Zhao, *Appl. Phys. Lett.* **2009**, *94*, 163104.

[14] A. A. Solovev, Y. Mei, E. B. Ureña, G. Huang, O. G. Schmidt, *Small* **2009**, *5*, 1688.

[15] W. Gao, S. Sattayasamitsathit, J. Orozco, J. Wang, *J. Am. Chem. Soc.* **2011**, *133*, 11862.

[16] P. H. Colberg, S. Y. Reigh, B. Robertson, R. Kapral, *Acc. Chem. Res.* **2014**, *47*, 3504.

[17] M. N. Popescu, S. Dietrich, M. Tasinkevych, J. Ralston, *Eur. Phys. J. E* **2010**, *31*, 351.

[18] A. Nourhani, P. E. Lammert, *Phys. Rev. Lett.* **2016**, *116*, 178302.

[19] W. Gao, A. Uygun, J. Wang, *J. Am. Chem. Soc.* **2011**, *134*, 897.

[20] S. N. Rasuli, R. Golestanian, *J. Phys. Condens. Matter* **2005**, *17*, S1171.

[21] H. R. Jiang, N. Yoshinaga, M. Sano, *Phys. Rev. Lett.* **2010**, *105*, 268302.

[22] L. Baraban, R. Streubel, D. Makarov, L. Han, D. Karnaushenko, O. G. Schmidt, G. Cuniberti, *ACS Nano* **2013**, *7*, 1360.

[23] B. Qian, D. Montiel, A. Bregulla, F. Cichos, H. Yang, *Chem. Sci.* **2013**, *4*, 1420.

[24] J. R. Gomez-Solano, A. Blokhuis, C. Bechinger, *Phys. Rev. Lett.* **2016**, *116*, 138301.

[25] S. T. Chang, V. N. Paunov, D. N. Petsev, O. D. Velev, *Nat. Mater.* **2007**, *6*, 235.

[26] L. Zhang, J. J. Abbott, L. Dong, K. E. Peyer, B. E. Kratochvil, H. Zhang, C. Bergeles, B. J. Nelson, *Nano Lett.* **2009**, *9*, 3663.

[27] S. Tottori, L. Zhang, F. Qiu, K. K. Krawczyk, A. Franco-Obregón, B. J. Nelson, *Adv. Mater.* **2012**, *24*, 811.

[28] S. Palagi, A. G. Mark, S. Y. Reigh, K. Melde, T. Qiu, H. Zeng, C. Parmeggiani, D. Martella, A. Sanchez-Castillo, N. Kapernaum, *Nat. Mater.* **2016**, *15*, 647.

[29] A. Ghosh, P. Fischer, *Nano Lett.* **2009**, *9*, 2243.

[30] a) M. Ibele, T. E. Mallouk, A. Sen, *Angew. Chem.* **2009**, *121*, 3358; b) *Angew. Chem. Int. Ed.* **2009**, *48*, 3308.

[31] L. Bouffier, V. Ravaine, N. Sojic, A. Kuhn, *Curr. Opin. Colloid Interface Sci.* **2016**, *21*, 57.

[32] a) D. Kagan, M. J. Benchimol, J. C. Claussen, E. Chuluun-Erdene, S. Esener, J. Wang, *Angew. Chem.* **2012**, *124*, 7637; b) *Angew. Chem. Int. Ed.* **2012**, *51*, 7519.

[33] W. Wang, L. A. Castro, M. Hoyos, T. E. Mallouk, *ACS Nano* **2012**, *6*, 6122.

[34] J. Wu, S. Balasubramanian, D. Kagan, K. M. Manesh, S. Campuzano, J. Wang, *Nat. Commun.* **2010**, *1*, 36.

[35] J. Orozco, A. Cortés, G. Cheng, S. Sattayasamitsathit, W. Gao, X. Feng, Y. Shen, J. Wang, *J. Am. Chem. Soc.* **2013**, *135*, 5336.

[36] W. Gao, X. Feng, A. Pei, J. Gu, J. Li, J. Wang, *Nanoscale* **2013**, *5*, 4696.

[37] L. Soler, V. Magdanz, V. M. Fomin, S. Sanchez, O. G. Schmidt, *ACS Nano* **2013**, *7*, 9611.

[38] B. Jurado-Sánchez, S. Sattayasamitsathit, W. Gao, L. Santos, Y. Fedorak, V. V. Singh, J. Orozco, M. Galarnyk, J. Wang, *Small* **2015**, *11*, 499.

[39] F. Mou, D. Pan, C. Chen, Y. Gao, L. Xu, J. Guan, *Adv. Funct. Mater.* **2015**, *25*, 6173.

[40] B. Dong, T. Zhou, H. Zhang, C. Y. Li, *ACS Nano* **2013**, *7*, 5192.

[41] S. Sundararajan, P. E. Lammert, A. W. Zudans, V. H. Crespi, A. Sen, *Nano Lett.* **2008**, *8*, 1271.

ADVANCED SCIENCE NEWS

www.advancedsciencenews.com

Particle
& Particle Systems Characterization

www.particle-journal.com

FULL PAPER

[42] A. A. Solovev, W. Xi, D. H. Gracias, S. M. Harazim, C. Deneke, S. Sanchez, O. G. Schmidt, *ACS Nano* **2012**, *6*, 1751.

[43] W. Gao, D. Kagan, O. S. Pak, C. Clawson, S. Campuzano, E. Chuluun-Erdene, E. Shipton, E. E. Fullerton, L. Zhang, E. Lauga, *Small* **2012**, *8*, 460.

[44] F. Mou, C. Chen, Q. Zhong, Y. Yin, H. Ma, J. Guan, *ACS Appl. Mater. Interfaces* **2014**, *6*, 9897.

[45] K. J. Rao, F. Li, L. Meng, H. Zheng, F. Cai, W. Wang, *Small* **2015**, *11*, 2836.

[46] W. Gao, R. Dong, S. Thamphiwatana, J. Li, W. Gao, L. Zhang, J. Wang, *ACS Nano* **2015**, *9*, 117.

[47] J. R. Baylis, J. H. Yeon, M. H. Thomson, A. Kazerooni, X. Wang, A. E. S. John, E. B. Lim, D. Chien, A. Lee, J. Q. Zhang, *Sci. Adv.* **2015**, *1*, e1500379.

[48] J. Wang, W. Gao, *ACS Nano* **2012**, *6*, 5745.

[49] L. K. Abdelmohsen, F. Peng, Y. Tu, D. A. Wilson, *J. Mater. Chem. B* **2014**, *2*, 2395.

[50] J. Wang, K. M. Manesh, *Small* **2010**, *6*, 338.

[51] W. Z. Teo, M. Pumera, *Chem. Eur. J.* **2016**, *22*, 1.

[52] J. Adler, *Science* **1966**, *153*, 708.

[53] G. J Dunderdale, S. Ebbens, *Curr. Phys. Chem.* **2015**, *5*, 91.

[54] R. D. Astumian, *ACS Nano* **2014**, *8*, 11917.

[55] A. R. Morgan, A. B. Dawson, H. S. Mckenzie, T. S. Skelhon, R. Beanland, H. P. Franks, S. A. Bon, *Mater. Horiz.* **2014**, *1*, 65.

[56] Y. Hong, N. M. Blackman, N. D. Kopp, A. Sen, D. Velegol, *Phys. Rev. Lett.* **2007**, *99*, 178103.

[57] a) L. Baraban, S. M. Harazim, S. Sanchez, O. G. Schmidt, *Angew. Chem.* **2013**, *125*, 5662; b) *Angew. Chem. Int. Ed.* **2013**, *52*, 5552.

[58] R. S. Rikken, R. J. Nolte, J. C. Maan, J. C. van Hest, D. A. Wilson, P. C. Christianen, *Soft Matter* **2014**, *10*, 1295.

[59] P. Fischer, A. Ghosh, *Nanoscale* **2011**, *3*, 557.

[60] P. L. Venugopalan, R. Sai, Y. Chandorkar, B. Basu, S. Shivashankar, A. Ghosh, *Nano Lett.* **2014**, *14*, 1968.

[61] F. Y. Cheng, C. H. Su, Y. S. Yang, C. S. Yeh, C. Y. Tsai, C. L. Wu, M. T. Wu, D. B. Shieh, *Biomaterials* **2005**, *26*, 729.

[62] Z. Wu, T. Li, J. Li, W. Gao, T. Xu, C. Christianson, W. Gao, M. Galarnyk, Q. He, L. Zhang, *ACS Nano* **2014**, *8*, 12041.

[63] K. K. Dey, K. K. Senapati, P. Phukan, S. Basu, A. Chattopadhyay, *J. Phys. Chem. C* **2011**, *115*, 12708.

[64] Y. C. Chao, W. H. Huang, K. M. Cheng, C. Kuo, *ACS Appl. Mater. Interfaces* **2014**, *6*, 4338.

[65] X. Yan, Q. Zhou, J. Yu, T. Xu, Y. Deng, T. Tang, Q. Feng, L. Bian, Y. Zhang, A. Ferreira, *Adv. Funct. Mater.* **2015**, *25*, 5333.

[66] P. Dhar, Y. Cao, T. Kline, P. Pal, C. Swayne, T. M. Fischer, B. Miller, T. E. Mallouk, A. Sen, T. H. Johansen, *J. Phys. Chem. C* **2007**, *111*, 3607.

[67] Z. Liu, Y. Liu, K. Yao, Z. Ding, J. Tao, X. Wang, *J. Mater. Synth. Process.* **2002**, *10*, 83.

[68] J. Wang, *Faraday Discuss.* **2013**, *164*, 9.

[69] Z. X. Sun, F. W. Su, W. Forsling, P. O. Samskog, *J. Colloid Interface Sci.* **1998**, *197*, 151.

[70] a) W. Wang, S. Li, L. Mair, S. Ahmed, T. J. Huang, T. E. Mallouk, *Angew. Chem.* **2014**, *126*, 3265; b) *Angew. Chem. Int. Ed.* **2014**, *53*, 3201.

[71] S. Ahmed, W. Wang, L. O. Mair, R. D. Fraleigh, S. Li, L. A. Castro, M. Hoyos, T. J. Huang, T. E. Mallouk, *Langmuir* **2013**, *29*, 16113.

[72] S. Ahmed, W. Wang, L. Bai, D. T. Gentekos, M. Hoyos, T. E. Mallouk, *ACS Nano* **2016**, *10*, 4763.

[73] V. Garcia-Gradilla, J. Orozco, S. Sattayasamitsathit, F. Soto, F. Kuralay, A. Pourazary, A. Katzenberg, W. Gao, Y. Shen, J. Wang, *ACS Nano* **2013**, *7*, 9232.

[74] F. Soto, G. L. Wagner, V. Garcia-Gradilla, K. T. Gillespie, D. R. Lakshmipathy, E. Karshalev, C. Angell, Y. Chen, J. Wang, *Nanoscale* **2016**, *8*, 17788.

[75] F. Nadal, E. Lauga, *Phys. Fluids* **2014**, *26*, 082001.

[76] R. Jain, D. Duda, *Vascular and Interstitial Biology of Tumors in Clinical Oncology*, Elsevier, Philadelphia, PA **2004**, p. 153.

[77] Y. Wang, R. M. Hernandez, D. J. Bartlett, J. M. Bingham, T. R. Kline, A. Sen, T. E. Mallouk, *Langmuir* **2006**, *22*, 10451.

[78] T. R. Kline, M. Tian, J. Wang, A. Sen, M. W. Chan, T. E. Mallouk, *Inorg. Chem.* **2006**, *45*, 7555.